© 2018. Published by The Company of Biologists Ltd | Journal of Cell Science (2018) 131, jcs218883. doi:10.1242/jcs.218883

RESEARCH ARTICLE

The topology of the lymphotoxin β receptor that accumulates upon endolysosomal dysfunction dictates the NF-κB signaling outcome

Magdalena Banach-Orłowska[1,*], Kamil Jastrzębski[1,*], Jarosław Cendrowski[1], Małgorzata Maksymowicz[1], Karolina Wojciechowska[1], Michał Korostyński[2], Dimitri Moreau[3], Jean Gruenberg[3] and Marta Miaczynska[1,‡]

ABSTRACT

Cytokine receptors, such as tumor necrosis factor receptor I (TNFRI, also known as TNFRSF1A) and lymphotoxin β receptor (LTβR), activate inflammatory nuclear factor (NF)-κB signaling upon stimulation. We have previously demonstrated that depletion of ESCRT components leads to endosomal accumulation of TNFRI and LTβR, and their ligand-independent signaling to NF-κB. Here, we studied whether other perturbations of the endolysosomal system could trigger intracellular accumulation and signaling of ligand-free LTβR. While depletion of the CORVET components had no effect, knockdown of Rab7a or HOPS components, or pharmacological inhibition of lysosomal degradation, caused endosomal accumulation of LTβR and increased its interaction with the TRAF2 and TRAF3 signaling adaptors. However, the NF-κB pathway was not activated under these conditions. We found that knockdown of Rab7a or HOPS components led to sequestration of LTβR in intraluminal vesicles of endosomes, thus precluding NF-κB signaling. This was in contrast to the LTβR localization on the outer endosomal membrane that was seen after ESCRT depletion and was permissive for signaling. We propose that the inflammatory response induced by intracellular accumulation of endocytosed cytokine receptors critically depends on the precise receptor topology within endosomal compartments.

KEY WORDS: Endocytosis, Endosome, HOPS complex, Rab7, NF-κB signaling

INTRODUCTION

Among other functions, endocytosis serves to maintain homeostasis of the plasma membrane and to downregulate receptors that perform signaling functions. The targeting of cell surface proteins for lysosome degradation is initiated at the plasma membrane by ubiquitin conjugation. Subsequently, ubiquitylated cargo is internalized into endosomes and recognized by subunits of the endosomal sorting complexes required for transport (ESCRT) (Christ et al., 2017; Frankel and Audhya, 2018). ESCRTs assemble on endosomal membranes and also drive the formation of intraluminal vesicles (ILVs), which contain the downregulated cargo. In parallel, early endosomes marked with Rab5 (which has Rab5a, Rab5b and Rab5c forms in mammals) mature into late endosomes positive for Rab7 (which has Rab7a and Rab7b forms in mammals) in a process known as Rab5-to-Rab7 conversion (Huotari and Helenius, 2011; Poteryaev et al., 2010; Rink et al., 2005; Scott et al., 2014). Finally, late endosomes fuse with lysosomes, where cargo is degraded. However, it is not clear how cargo sorting for degradation is coordinated with endosomal membrane dynamics. In the endosomal system, docking/fusion depends on two tethering complexes: the class C core vacuole/endosome tethering (CORVET), and homotypic fusion and protein sorting (HOPS) complexes, which in yeast are recruited by Rab5 and Rab7, respectively (Balderhaar and Ungermann, 2013; Spang, 2016). In mammalian cells, HOPS does not interact with Rab7 but is recruited to membranes via interaction with Arl8b and RILP (Khatter et al., 2015; Lin et al., 2014). Both CORVET and HOPS complexes are composed of six subunits, with four (Vps11, Vps16, Vps18 and Vps33A) being shared between them. The complexes differ by two subunits: Vps3 (also known as TGFBRAP1 or TRAP1) and Vps8 in CORVET, versus Vps39 and Vps41 in HOPS (Markgraf et al., 2009; Peplowska et al., 2007; Price et al., 2000).

Endocytic internalization and trafficking can regulate the signal transduction of plasma membrane receptors in multiple ways. These include termination of signaling through lysosomal degradation of receptors but also maintenance of signaling by retention of active receptors on endosomes (Barbieri et al., 2016; Miaczynska, 2013; Szymanska et al., 2018; Villasenor et al., 2016). While our knowledge of mechanisms linking trafficking and signaling comes mostly from research on receptor tyrosine kinases or G protein-coupled receptors, less is known about cytokine receptors of the tumor necrosis factor receptor (TNFR) superfamily (Cendrowski et al., 2016). Of the latter class, we focused on lymphotoxin β receptor (LTβR), which is activated by membrane-bound ligands lymphotoxin α1β2 or LIGHT (also known as TNFSF14) (Remouchamps et al., 2011). In contrast to a relatively broad expression pattern of the receptor, the expression of its ligands is restricted to lymphocytes (B, T and NK cells). Upon stimulation, LTβR recruits cytoplasmic TNFR-associated factor (TRAF) adaptors (Kim et al., 2005; Nakano et al., 1996; VanArsdale et al., 1997) and activates both the canonical and non-canonical nuclear factor (NF)-κB pathways (Dejardin et al., 2002; Müller and Siebenlist, 2003). Further downstream, the canonical pathway is driven by degradation of IκBα (NFKBIA) inhibitor, followed by phosphorylation and nuclear translocation of NF-κB transcription factor RelA. The non-canonical branch involves processing of p100 NF-κB precursor (encoded by *NFKB2*) to the transcriptionally active p52 form (Zhang et al., 2017).

While the signaling pathways mediated by LTβR are well established, its trafficking routes are less studied. Ligand-induced LTβR has been reported to undergo dynamin-mediated internalization that is linked to the activation of non-canonical NF-κB signaling

[1]Laboratory of Cell Biology, International Institute of Molecular and Cell Biology, 02-109, Warsaw, Poland. [2]Department of Molecular Neuropharmacology, Institute of Pharmacology Polish Academy of Sciences, 31-343, Krakow, Poland. [3]Department of Biochemistry, University of Geneva, 1211, Geneva, Switzerland. *These authors contributed equally to this work

‡Author for correspondence (miaczynska@iimcb.gov.pl)

M.B.-O., 0000-0003-0617-109X; K.J., 0000-0001-6481-1759; J.C., 0000-0002-8579-7279; M. Maksymowicz, 0000-0002-8487-5845; K.W., 0000-0002-8220-6357; M. Miaczynska, 0000-0003-0031-5267

Received 10 April 2018; Accepted 8 October 2018

Journal of Cell Science (2018) 131, jcs218883. doi:10.1242/jcs.218883

(Ganeff et al., 2011). However, most cell types do not express LTβR ligands. We have recently shown that, at steady-state, HEK 293 cells contain an intracellular pool of ligand-free LTβR that largely overlaps with endosomal markers EEA1 or LAMP1, with over 30% colocalization with either marker (Maminska et al., 2016). Importantly, accumulation of ligand-free LTβR on endosomes markedly increases upon depletion of ESCRT-I components, which interferes with cargo sorting into ILVs and cargo lysosome targeting. Under these conditions, local oligomerization and activation of LTβR trigger canonical and non-canonical NF-κB signaling from endosomes in a ligand-independent manner (Maminska et al., 2016). However, it remained unclear whether other perturbations of the endosomal system also lead to an increased intracellular accumulation of LTβR as well as inflammatory NF-κB signaling in cells that do not express LTβR ligands. In this study, we investigated whether dysfunction of the other endosomal complexes involved in endosome maturation, namely CORVET and HOPS, affected trafficking and signaling of ligand-free LTβR. We show that depletion of Rab7a (hereafter referred to as Rab7) or HOPS caused accumulation of the receptor on endosomes but, in contrast to what was seen upon ESCRT knockdown, without induction of the NF-κB pathway. We propose that different effects of ESCRT or HOPS depletion on inflammatory signaling result from the different topology of the ligand-free LTβR that accumulated in endosomes under both conditions.

RESULTS

HOPS but not CORVET regulates intracellular trafficking of LTβR

To assess the involvement of CORVET and HOPS complexes in trafficking of ligand-free LTβR, we depleted their two shared core subunits, Vps16 and Vps18 (Fig. 1A–E), and assessed the intracellular distribution of LTβR in HeLa cells via confocal microscopy. When compared to control cells (transfected with non-targeting siRNAs), cells deprived of either subunit exhibited stronger vesicular staining of LTβR (Fig. 1A). We quantitatively analyzed the images with respect to integral (also known as integrated) fluorescence intensity of EEA1-, LAMP1- or LTβR-positive vesicles, as the parameter that represents the amount of a particular protein localized to vesicular structures (Fig. 1B,C). Moreover, for LTβR, we calculated its concentration per vesicle (represented by mean of integral fluorescence intensity) (Fig. 1C) and colocalization of the receptor with endosomal markers upon Vps16 or Vps18 depletion (Fig. 1D). In general, quantitative image analysis revealed no substantial changes in the integral intensity of EEA1- or LAMP1-positive vesicles. Importantly, both total amounts and concentration of LTβR per vesicle were increased under these conditions (Fig. 1C), although LTβR colocalization with early or late endosome markers was not affected (Fig. 1D). Nevertheless, these data allowed us to conclude that the disruption of CORVET and/or HOPS complexes leads to the vesicular accumulation of LTβR.

To discriminate which of the two complexes was required for the regulation of LTβR trafficking we knocked down expression of their specific subunits. We found that neither the general distribution of LTβR nor its amounts and concentration on endosomes were affected upon depletion of the CORVET subunits Vps3 and Vps8 (Fig. S1A,B). Their silencing was efficient (Fig. S1C) and led to increased colocalization of transferrin with EEA1 (Fig. S1D), as previously reported (Perini et al., 2014). We conclude that CORVET is functional in our cellular model; however, it is dispensable for LTβR sorting.

Next, we investigated whether HOPS was involved in intracellular transport of LTβR. To this end, we depleted the unique subunits of this complex, Vps39 and Vps41, as well as another shared HOPS/CORVET subunit, Vps11 (Fig. 2A–E). The integral intensity of EEA1- but not LAMP1-positive endosomes was increased in these cells (Fig. 2B). In agreement with the data from Vps16- and Vps18-depleted cells (Fig. 1A,C), we also found a higher endosomal accumulation of LTβR upon Vps11, Vps39 and Vps41 silencing (Fig. 2A,C). Interestingly, colocalization of LTβR on vesicles positive for both LAMP1 and EEA1 was increased (Fig. 2D), suggesting that LTβR accumulates on aberrant endosomes simultaneously bearing both markers. The observed change in LTβR cellular distribution after depletion of Vps39, Vps41 or Vps11 was not accompanied by a significant change in LTβR abundance, as measured by immunoblotting (Fig. 2F). This implies that LTβR is re-localized in cells upon depletion of HOPS components.

To exclude possible off-target effects of siRNA, we examined heterogeneous (see later) HeLa cell lines with depletion of Vps39 or Vps41 that had been prepared with a CRISPR/Cas9 approach. For each protein, we used two independent single-guide RNA (sgRNA) sequences. Parental HeLa cells were employed as a control. Similar to what was seen with siRNA for Vps39 and Vps41, we observed changes in the distribution of LTβR and endosomal markers (Fig. S2A–C). The values of both the integral and mean fluorescence intensity of LTβR were higher (Fig. S2C), and colocalization of the receptor with LAMP1 and EEA1 was increased in CRISPR-modified cells (Fig. S2D), as it was upon siRNA-mediated HOPS depletion (Fig. 2C,D). These effects were clearly measureable despite the modest efficiency of depletion mediated by sgRNA, which was likely due to heterogeneity in the investigated pools of cells (Fig. S2E,F).

Taken together, these data indicate that trafficking of ligand-free LTβR engages the HOPS tethering complex but not CORVET. These observations also suggest that, although the two complexes share a common core, their functions can be uncoupled, with CORVET possibly playing a more-specialized role in the transport of certain cargoes.

Rab7 regulates trafficking and degradation of LTβR

The HOPS complex in yeast is recruited to endosomal membranes by Rab7 (Balderhaar and Ungermann, 2013; Spang, 2016). In mammalian cells, the role of Rab7 in this process is still unclear (Guerra and Bucci, 2016). However, Rab7 is a key regulator of the transition from early to late endosomes and could potentially regulate LTβR trafficking. To evaluate this, we investigated the intracellular distribution of the receptor by confocal microscopy in cells transfected with two independent siRNAs (Fig. 3A–D) or one shRNA targeting Rab7 (Fig. S3A–C). We found that Rab7 depletion affected the distribution of LTβR (Fig. 3A,C; Fig. S3A,B) and EEA1 (Fig. 3A,B). Quantitative analysis of images revealed that both the amounts and the concentration of LTβR on vesicles were increased (Fig. 3C; Fig. S3B). Moreover, similar to what was seen upon HOPS depletion, Rab7 removal resulted in higher amounts of EEA1 on endosomes without affecting LAMP1-marked vesicles (Fig. 3A,B) and led to increased colocalization of the receptor with EEA1 and LAMP1 (Fig. 3D).

To further confirm the role of Rab7 as a regulator of LTβR trafficking, we performed rescue experiments via overexpression of canine Rab7 tagged with HA. As a control, we used an empty pcDNA3 plasmid encoding HA. As expected, in cells transfected with Rab7_2 siRNA and Rab7 plasmid (resistant to this siRNA), we could observe expression of canine Rab7 protein, visualized by

Journal of Cell Science (2018) 131, jcs218883. doi:10.1242/jcs.218883

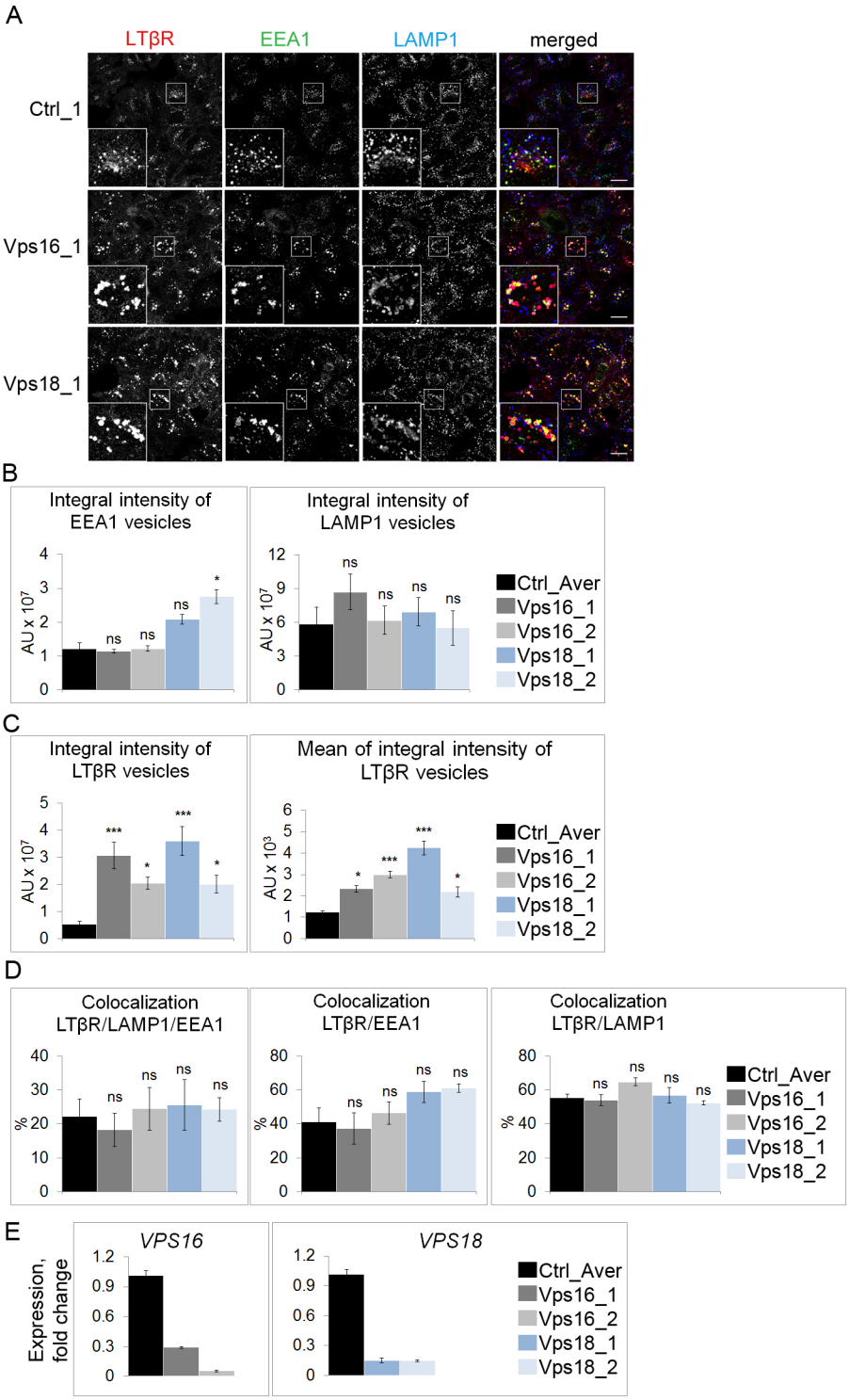

Fig. 1. Depletion of shared HOPS and CORVET components affects the intracellular distribution of LTβR. (A) Immunofluorescence staining of LTβR, EEA1 and LAMP1 in HeLa cells upon knockdown of Vps16 or Vps18 and in control (Ctrl) siRNA-transfected cells. Insets show magnified views of the regions boxed in the main images. Scale bars: 20 µm. (B) Analysis of integral intensities of EEA1- and LAMP1-positive vesicles in cells depleted of Vps16 or Vps18 (two independent siRNA oligonucleotides per gene). (C) Analysis of integral and mean of integral intensities of LTβR-positive vesicles in cells depleted of Vps16 or Vps18 (as above). (D) Analysis of colocalization between LTβR, LAMP1 and EEA1; LTβR and EEA1; and LTβR and LAMP1 in cells depleted of Vps16 or Vps18 (as above). (E) qRT-PCR analysis of the silencing efficiency of *VPS16* or *VPS18* in HeLa cells. Black bars (Ctrl_Aver) in B–E represent values averaged for two non-targeting siRNAs transfected independently (Ctrl_1 and Ctrl_2). Data represent the means±s.e.m., n=4 (B), n≥3 (C), n=4 (D) and n=3 (E). *P≤0.05; ***P≤0.001; ns, not significant (P>0.05) (ANOVA or Kruskal–Wallis test).

HA staining (Fig. 3E), and significant reduction of the vesicular accumulation of LTβR in comparison to that measured in cells co-transfected with Rab7_2 siRNA and empty pcDNA plasmid with HA (Fig. 3F). As an additional control, we saw no expression of HA–Rab7 in cells transfected with Rab7_1 siRNA (fully matching the canine Rab7 sequence) and the high levels of endosomal LTβR accumulation remained unchanged (Fig. 3E,F).

As the analysis of microscopy data showed elevated amounts and concentration of the receptor on vesicles in Rab7-depleted cells, we measured the total abundance of LTβR by immunoblotting. In contrast to what was seen upon the depletion of HOPS components, Rab7 knockdown caused a statistically significant increase in total receptor levels (Fig. 3G), implying that LTβR degradation was impaired under these conditions.

Cumulatively, our findings suggest that ligand-free LTβR can be constitutively endocytosed and sorted to lysosomes in a process involving Rab7. While the requirement for Rab7 appears to be critical for efficient LTβR degradation, depletion of HOPS (Fig. 2F)

Journal of Cell Science (2018) 131, jcs218883. doi:10.1242/jcs.218883

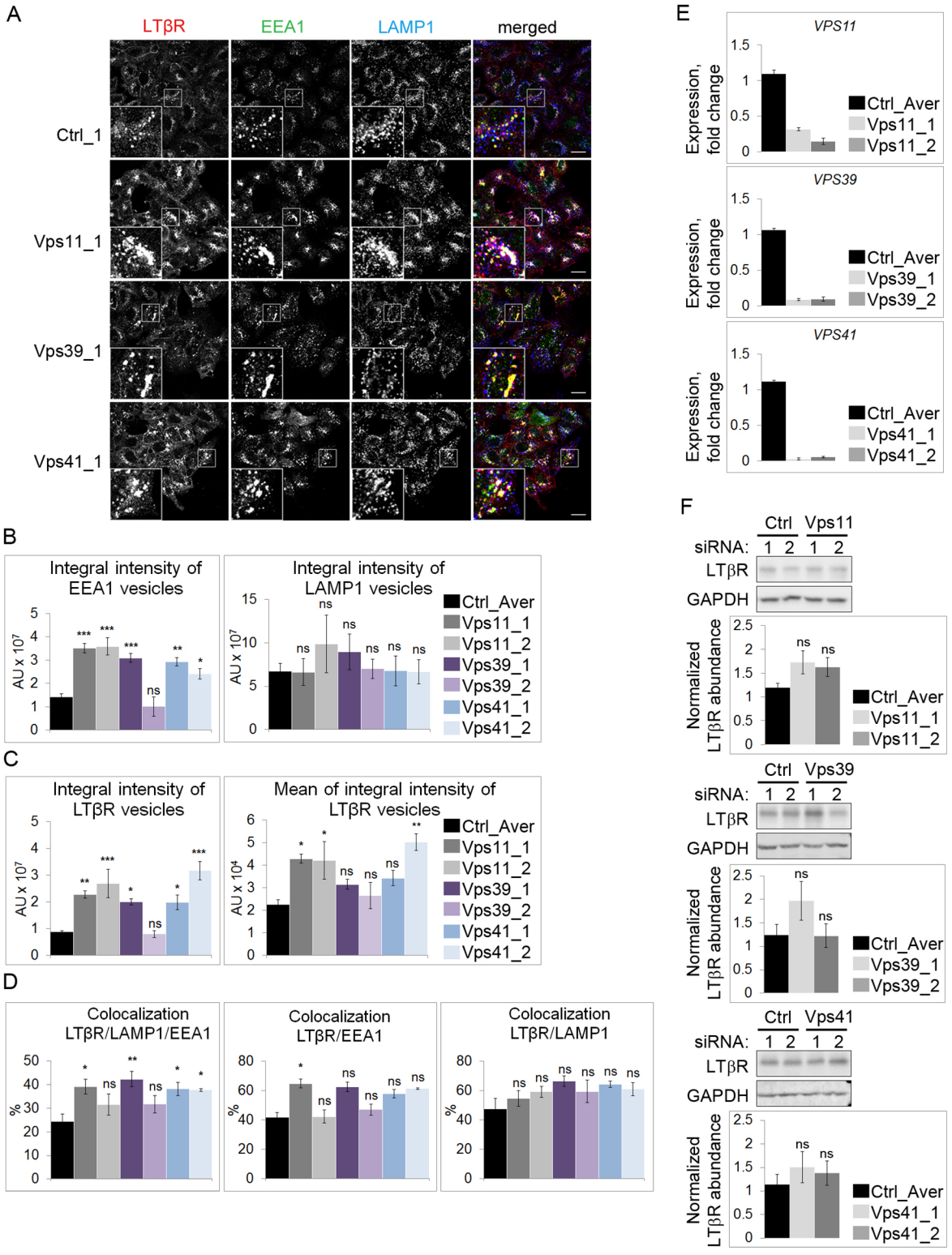

Fig. 2. Depletion of HOPS complex leads to endosomal accumulation of LTβR. (A) Immunofluorescence staining of LTβR, EEA1 and LAMP1 in HeLa cells upon knockdown of the indicated HOPS components or in control (Ctrl) siRNA-transfected cells. Insets show magnified views of the regions boxed in the main images. Scale bars: 20 µm. (B) Analysis of integral intensities of EEA1- and LAMP1-positive vesicles in cells with HOPS knockdown (two independent siRNA oligonucleotides per gene). (C) Analysis of integral and mean of integral intensities of LTβR-positive vesicles in cells with HOPS knockdown (as above). (D) Analysis of colocalization between LTβR, LAMP1 and EEA1; LTβR and EEA1; and LTβR and LAMP1 in cells depleted of the indicated HOPS components. The color code is as in B and C. (E) qRT-PCR analysis of the silencing efficiency of *VPS11*, *VPS39* or *VPS41* in HeLa cells. (F) Lysates of HeLa cells depleted of the indicated HOPS subunits were analyzed by western blotting with antibodies against LTβR, with GAPDH used as a loading control. Graphs depict the quantification of LTβR abundance. Black bars (Ctrl_Aver) in B–F represent values averaged for two non-targeting siRNAs transfected independently (Ctrl_1 and Ctrl_2). Data represent the means±s.e.m., n=4 (B), n=4 (C), n=3 (D), n=3 (E) and $n\geq3$ (F). *$P\leq0.05$; **$P\leq0.01$; ***$P\leq0.001$; ns, not significant ($P>0.05$) (ANOVA or Kruskal–Wallis test).

Journal of Cell Science

Journal of Cell Science (2018) 131, jcs218883. doi:10.1242/jcs.218883

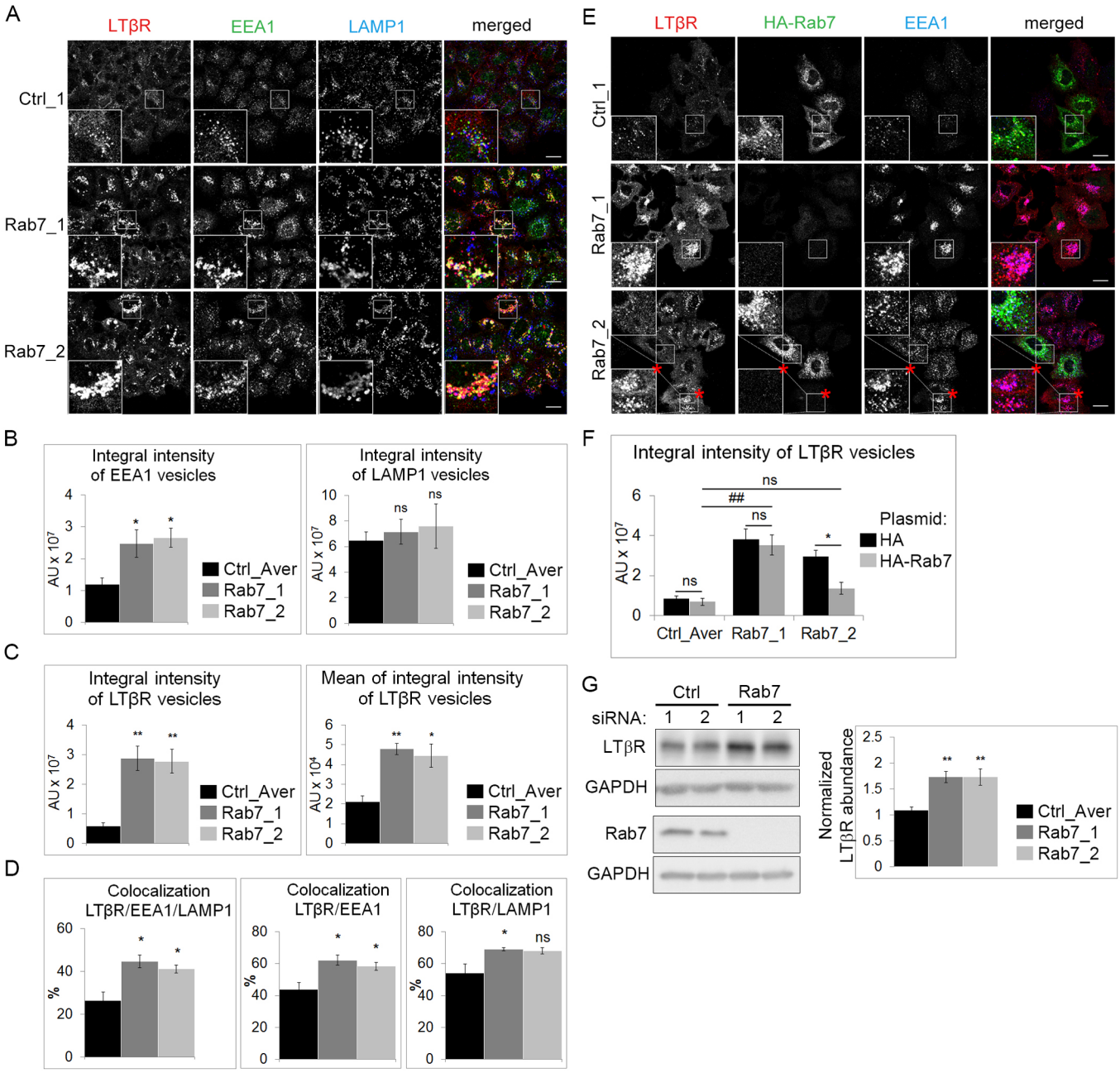

Fig. 3. Depletion of Rab7 causes endosomal accumulation of LTβR and increases the total level of the receptor. (A) Immunofluorescence staining of LTβR, EEA1 and LAMP1 in HeLa cells upon knockdown of Rab7 or in control (Ctrl) siRNA-transfected cells. Insets show magnified views of the regions boxed in the main images. Scale bars: 20 µm. (B) Analysis of integral intensities of EEA1- and LAMP1-positive vesicles in cells depleted of Rab7 with two independent siRNA oligonucleotides. (C) Analysis of integral and mean of integral intensities of LTβR-positive vesicles in cells depleted of Rab7 (as above). (D) Analysis of colocalization between LTβR, LAMP1 and EEA1; LTβR and EEA1; and LTβR and LAMP1 in cells depleted of Rab7 (as above; color code as in B and C). (E) Immunofluorescence staining of LTβR, HA-tagged Rab7 and EEA1 in HeLa cells transfected with Rab7-targeting or control non-targeting (Ctrl) siRNAs, and the plasmid encoding a HA-Rab7 fusion protein resistant to Rab7_2 siRNA but sensitive to Rab7_1 siRNA. Insets show magnified views of the regions boxed in the main images. Scale bars: 20 µm. The asterisk marks cells not transfected with HA–Rab7. (F) Analysis of integral intensity of LTβR-positive vesicles in HeLa cells transfected with Rab7-targeting or control non-targeting (Ctrl) siRNAs (two independent oligonucleotides in each case), and the plasmid encoding a HA–Rab7 fusion or control plasmid encoding the HA tag. (G) Lysates of HeLa cells depleted of Rab7 were analyzed by western blotting with antibodies against LTβR or Rab7, with GAPDH used as a loading control. Graph depicts quantification of LTβR abundance upon Rab7 knockdown. Black bars (Ctrl_Aver) in B–D and G represent values averaged of two non-targeting siRNAs transfected independently (Ctrl_1 and Ctrl_2). Data represent the means±s.e.m., n=4 (B), n=3 (C), n=3 (D), n=3 (F) and n=4 (G). *$P\leq0.05$; $^{\#\#,**}P\leq0.01$; ns, not significant ($P>0.05$) (ANOVA or Student's t-test).

or ESCRT (Maminska et al., 2016) does not change abundance of LTβR. This may point to the existence of some compensatory or by-pass mechanisms for elimination of excess LTβR (e.g. via alternative routes to lysosomal degradation) when these complexes are dysfunctional.

Rab7- and Vps11-depleted cells show increased LTβR–TRAF association that does not activate the NF-κB pathway

The increased accumulation of LTβR on endosomes upon depletion of Rab7 or HOPS components prompted us to test whether the receptor is in an active state and induces NF-κB

Journal of Cell Science

Journal of Cell Science (2018) 131, jcs218883. doi:10.1242/jcs.218883

signaling from endosomes, as it does upon ESCRT depletion (Maminska et al., 2016). A prerequisite for the NF-κB pathway activation is the recruitment of TRAF adaptor proteins to oligomerized LTβR that occurs upon ligand stimulation, or, as we previously demonstrated, upon ESCRT dysfunction in the absence of ligands (Maminska et al., 2016). We thus measured the interaction between LTβR and TRAF2 and/or TRAF3 proteins by performing immunoprecipitation from lysates of cells transfected with control siRNAs or siRNAs targeting Rab7, or the representative HOPS subunit Vps11. Fig. 4A shows that there were greatly increased amounts of TRAF2 and TRAF3 that co-immunoprecipitated with LTβR in cells with knockdown of Rab7 or Vps11. Since Rab7-deprived cells contain more LTβR, we quantified the ratio of co-immunoprecipitated TRAF2 to immunoprecipitated LTβR. Even after such normalization, there was a significantly higher level of LTβR–TRAF2 complexes formed upon Rab7 or Vps11 knockdown than in control cells (graph in Fig. 4A). In addition, total TRAF2 or TRAF3 levels were not changed upon Rab7 or Vps11 knockdown (Fig. S4A).

These results suggest that, in cells depleted of Rab7 or HOPS components, LTβR is activated and able to trigger NF-κB signaling. We thus assessed the activity of both the canonical and non-canonical branches of the NF-κB pathway by measuring the status of their effector proteins. Surprisingly, Rab7 or HOPS depletion had no effect on the phosphorylation of RelA or the levels of the pathway inhibitor IκBα (both hallmarks of the canonical branch), nor on p100 processing into active p52 (a hallmark of the non-canonical branch) (Fig. 4B,C). In contrast, knockdown of the ESCRT-I component Vps28 activated the NF-κB pathway (Fig. 4D), as previously shown (Maminska et al., 2016).

Since it is known that LTβR can also induce JNK signaling (Chang et al., 2002; Kim et al., 2005), we examined its status upon depletion of Rab7, HOPS or ESCRT but did not detect active phosphorylated form of JNK (Fig. S4B,C), although JNK signaling could be induced in HeLa cells by addition of agonistic antibody for LTβR (Fig. S4D). We also monitored phosphorylation of Akt proteins and Erk1 and Erk2 (Erk1/2; also known as MAPK3 and MAPK1), which are commonly activated in response to the stimulation of membrane receptors. We found that depletion of HOPS components or Rab7 did not induce these signaling pathways (Fig. S4B,C). Increased phosphorylation of Erk1/2 was only observed upon ESCRT depletion (Fig. S4C), which was previously shown to enhance EGF-induced Erk1/2 activation (Brankatschk et al., 2012).

In parallel to biochemical analyses, we examined the effect of HOPS or Rab7 depletion at the transcriptional level. Quantitative real-time RT-PCR (qRT-PCR) analysis confirmed that there was no activation of selected NF-κB target genes (Fig. S5A). The increased *TNF* or *RELB* expression seen with some single siRNAs (Vps11_1, Rab7_2) was not reproduced by other reagents and probably reflected unspecific off-target effects. In contrast, Vps28 depletion potently induced expression of four out of six selected target genes, *IL8* (also known as *CXCL8*), *TNF*, *ICAM1* and *NFKBIA* (Fig. S5B), in line with our biochemical analysis (Fig. 4D) and our previous study (Maminska et al., 2016). Taken together, these data show that, in HeLa cells, the NF-κB pathway is not activated upon Rab7 or HOPS depletion, despite robust interactions of LTβR with its signaling TRAF adaptors.

Since we had previously shown that the NF-κB pathway was very strongly activated upon ESCRT silencing in HEK 293 cells (Maminska et al., 2016), we repeated our experiments in these cells as an additional control. We again found that knockdown of HOPS components did not affect the transcription of NF-κB target genes (Fig. S5C), while depletion of Vps28 induced a very potent inflammatory transcriptional response (Fig. S5D).

Finally, to assess whether, instead of NF-κB, other intracellular signaling pathways are affected by HOPS knockdown, we analyzed the transcriptome of HEK 293 cells depleted of Vps11, Vps39 or Vps41. We found no pronounced changes in a general expression profile of HEK 293 cells transfected with siRNAs targeting the HOPS components (Fig. S5E). We did not detect any transcriptional signature of particular signaling pathways among 108 significantly up-regulated genes, which encoded mainly plasma membrane or secreted proteins. Hence, the lack of a signaling response after depletion of Vps11, Vps39 or Vps41 in both HeLa and HEK 293 cell lines demonstrates that the endosomal accumulation of LTβR is clearly not sufficient to activate NF-κB signaling. Furthermore, in contrast to ESCRT dysfunction (Brankatschk et al., 2012; Maminska et al., 2016), inactivation of HOPS has no major impact on the cellular transcriptional program.

Inhibition of lysosomal degradation leads to endosomal accumulation of LTβR and its increased binding to TRAF proteins without activating the NF-κB pathway

To further corroborate our findings, we employed a pharmacological approach to inhibit lysosomal degradation and check its impact on LTβR trafficking and activation. To this end, we used chloroquine, which prevents acidification of endosomal compartments and thus inhibits the activity of lysosomal enzymes. Chloroquine treatment of HeLa cells did not change integral fluorescence intensity of EEA1 or LAMP1 vesicles (Fig. 5A,B), but significantly increased both the amounts and concentration of LTβR on vesicles, which predominantly colocalized with LAMP1 (Fig. 5A,C,D). This may indicate that, under these conditions, the receptor accumulates in late endosomes/lysosomes, rather than in the aberrant vesicles marked with LAMP1 and EEA1 as occurs upon depletion of HOPS or Rab7. We verified, by immunoblotting analyses, that the total levels of LTβR were increased (Fig. 5E) pointing to an impairment of lysosomal degradation of the receptor in chloroquine-treated cells. Importantly, NF-κB signaling was not activated under these conditions (Fig. 5E), although the receptor strongly interacted with TRAF proteins (Fig. 5F). These data demonstrate that the chloroquine treatment phenocopies the effects of Rab7 depletion. In both cases, inhibition of lysosomal degradation results in the accumulation of LTβR bound to its signaling adaptor without induction of the NF-κB pathway.

The topology of LTβR accumulated on EEA1-positive endosomes in cells depleted of HOPS or defective in lysosomal degradation is different than in ESCRT-depleted cells

Next, we investigated why the NF-κB signaling outcome is different in cells depleted of ESCRT-I versus HOPS or Rab7. In both cases, LTβR accumulates intracellularly on endosomes in an active state, as it is strongly associated with its signaling TRAF adaptors. In ESCRT-depleted cells, this leads to pronounced NF-κB activation and inflammatory signaling, while upon HOPS or Rab7 knockdown (or chloroquine treatment) signaling is not induced. We hypothesized that different suborganellar localization of LTβR within endosomes may account for these differences. Specifically, as ESCRTs regulate the formation of ILVs on endosomes, we predicted that ESCRT-I depletion would lead to the accumulation of LTβR on the outer limiting membrane of enlarged endosomes. In this case, the intracellular part of the receptor would be exposed to the cytoplasm and could interact with components of the NF-κB pathway. In contrast, in HOPS- or Rab7-depleted cells, or in cells treated with

Journal of Cell Science (2018) 131, jcs218883. doi:10.1242/jcs.218883

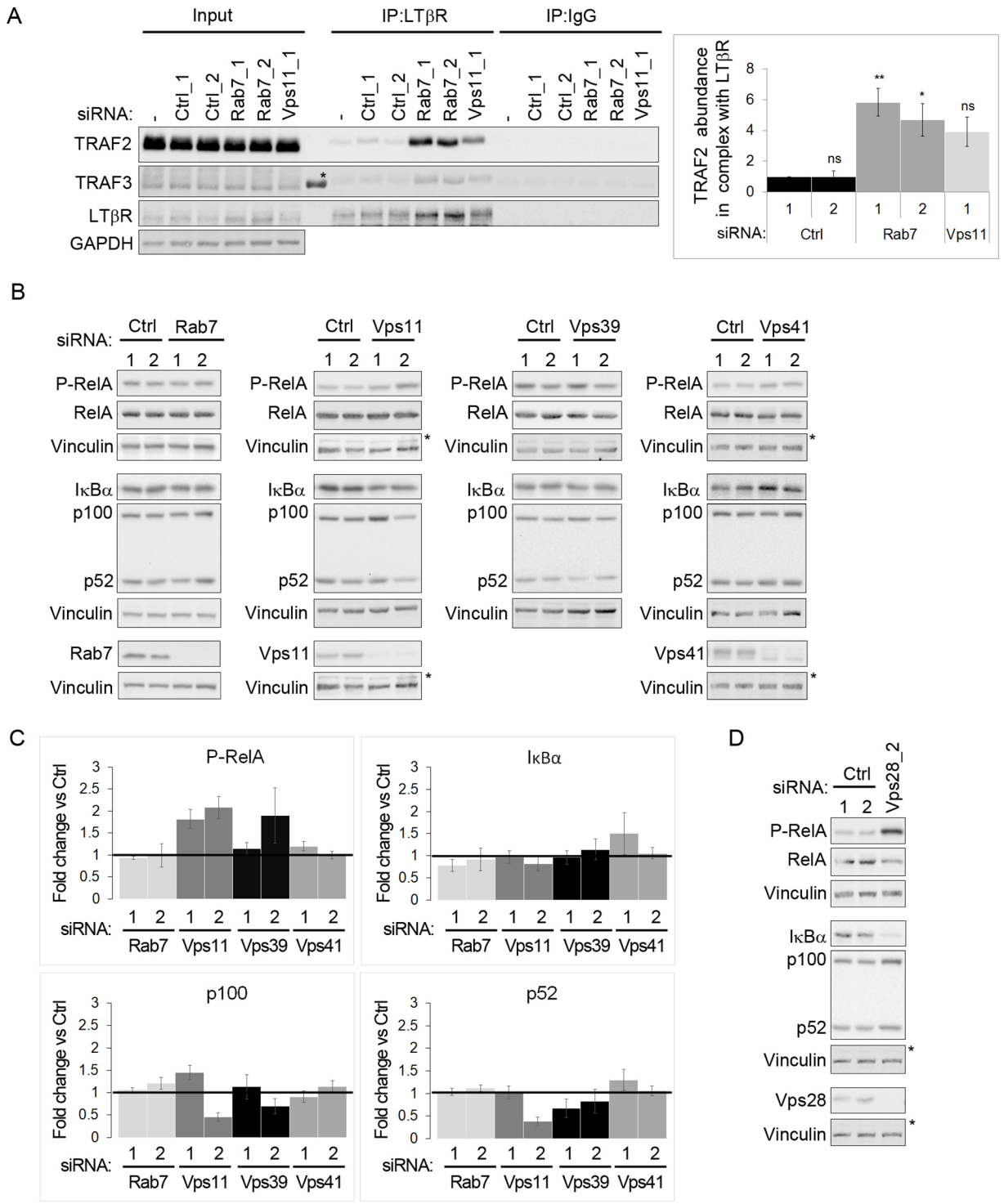

Fig. 4. Rab7- and Vps11-depleted cells show increased LTβR-TRAF association that does not activate the NF-κB pathway. (A) Left panel, western blot analysis of immunoprecipitation (IP) of LTβR in extracts of HeLa cells transfected with non-targeting (Ctrl) or Rab7- and Vps11-targeting siRNA. Antibodies against LTβR, TRAF2 and TRAF3 were used for immunoblotting, with GAPDH as a loading control. The input represents 10% of lysates used for IP. An asterisk marks an unspecific band in the molecular mass markers. Right panel, the TRAF2 abundance in LTβR immunoprecipitates upon knockdown of Rab7 and Vps11 was quantified as a ratio of co-immunoprecipitated TRAF2 to immunoprecipitated LTβR. Data were normalized to the TRAF2:LTβR ratio in Ctrl_1 siRNA-transfected cells, which was assigned a value of 1. Data represent the means±s.e.m., n=3. *P≤0.05; **P≤0.01; ns, not significant (P>0.05) (ANOVA test). (B,D) Lysates of HeLa cells depleted of Rab7 and HOPS subunits (B) or ESCRT-I subunit Vps28 (D) were analyzed by western blotting with antibodies against the indicated markers of NF-κB activation and the depleted proteins, with vinculin as a loading control. Blots are representative of three experiments. Asterisks indicate the same blots of vinculin within each panel, presented twice for clarity. Knockdown efficiency of Vps39 was tested by qRT-PCR as shown in Fig. 2E, as no available antibody worked for western blotting. P-RelA, phosphorylated RelA. (C) Abundance of P-RelA, IκBα, p100 and p52 proteins in extracts of Hela cells transfected with siRNAs targeting Rab7 and HOPS subunits as analyzed by western blotting (representative blots shown in B), quantified and presented as a fold change versus Ctrl_ Aver (averaged Ctrl_1 and Ctrl_2), which was assigned a value of 1. Data represent the means±s.e.m., n≥3, except Vps41_1 (n=2).

Journal of Cell Science

Journal of Cell Science (2018) 131, jcs218883. doi:10.1242/jcs.218883

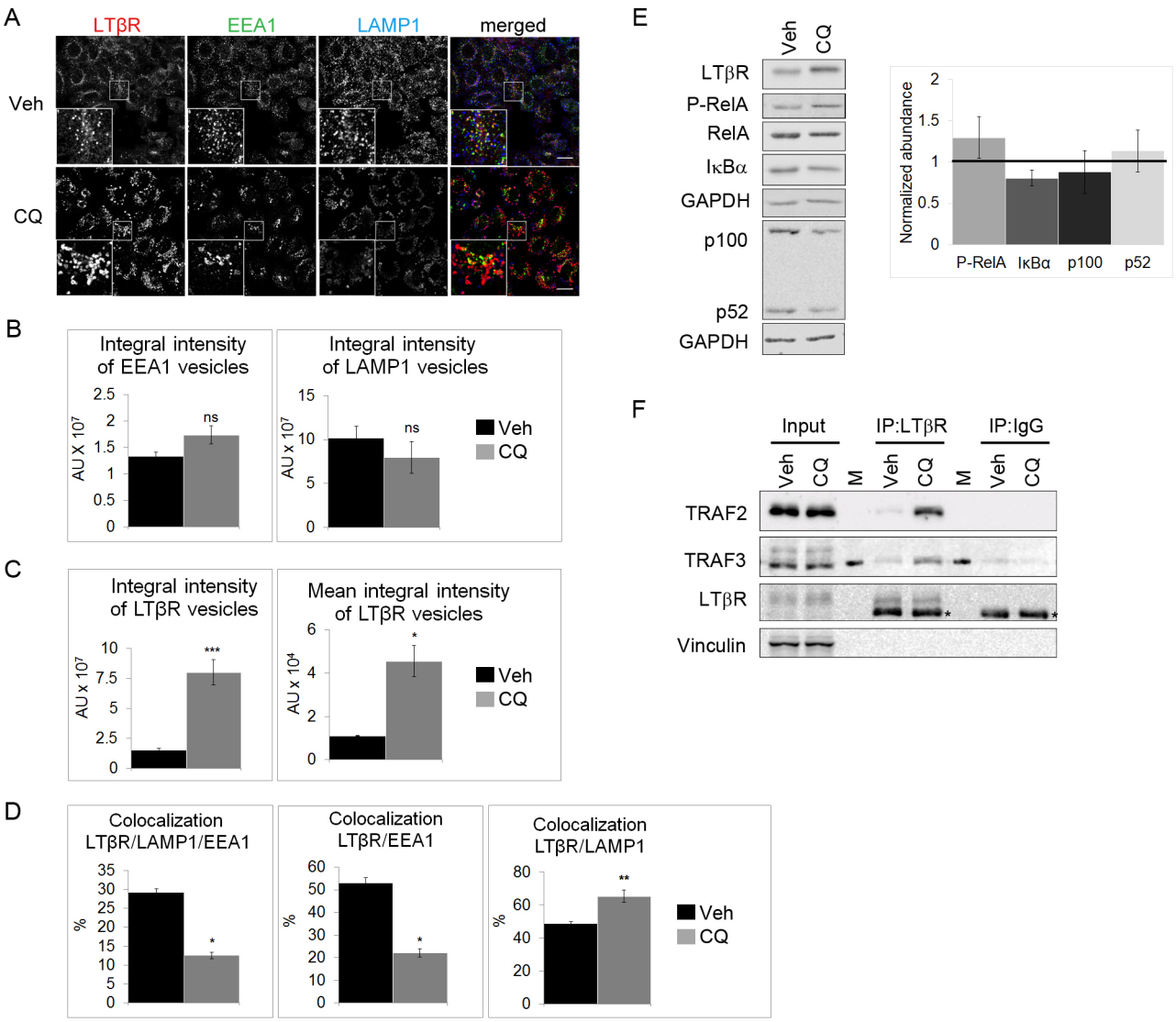

Fig. 5. Inhibition of lysosomal degradation leads to endosomal accumulation of LTβR and its increased binding to TRAF proteins without activating the NF-κB pathway. (A) Immunofluorescence staining of LTβR, EEA1 and LAMP1 in HeLa cells treated with lysosomal inhibitor chloroquine (CQ) or vehicle (Veh). Insets show magnified views of the regions boxed in the main images. Scale bars: 20 µm. (B–D) Analysis of integral intensities of EEA1- and LAMP1-positive vesicles (B), integral and mean of integral intensities of LTβR-positive vesicles (C), colocalization between LTβR, LAMP1 and EEA1; LTβR and EEA1; and LTβR and LAMP1 (D) in cells treated with CQ or vehicle (Veh). Data represent the means±s.e.m., n=4. *P≤0.05; **P≤0.01; ***P≤0.001 (Student's t-test). (E) Lysates of HeLa cells treated with CQ or vehicle (Veh) were analyzed by western blotting with antibodies against the indicated markers of NF-κB activation, with GAPDH as a loading control. P-RelA, phosphorylated RelA. Blots are representative of three experiments. Right graph, the abundance of P-RelA, IκBα, p100 and p52 proteins in HeLa cells treated with CQ was quantified and presented as a fold change versus control (Veh), which was assigned a value of 1. Data represent the means±s.e.m., n=3. (F) Western blot analysis of immunoprecipitation (IP) of LTβR from extracts of HeLa cells treated with CQ or vehicle. Antibodies against LTβR, TRAF2 and TRAF3 were used for blotting, with vinculin as a loading control. Input represents 10% of lysates used for IP. Asterisks mark heavy chain of antibodies used for IP. Blots are representative of two experiments. M, lane loaded with molecular mass marker.

chloroquine, LTβR would not be degraded but would instead be sequestered inside properly formed ILVs, from where it could not transduce NF-κB signaling to the cytoplasm.

To verify this hypothesis, we investigated the topology of LTβR on endosomes by using Airyscan microscopy, which provides higher resolution images than regular confocal microscopy. In ESCRT-depleted cells, LTβR was found on the outer membrane of enlarged vesicles, where it colocalized with EEA1, which resides on the cytoplasmic leaflet of the endosomal membrane (Fig. 6A). Upon HOPS depletion, the accumulated receptor localized inside the lumen of enlarged endosomes and showed only limited colocalization with EEA1 (Fig. 6A). A similar phenotype was observed in cells with Rab7 knockdown (Fig. 6A) or treated with chloroquine (Fig. 6B).

To further investigate the differences in the endosomal topology of LTβR in ESCRT- versus HOPS- or Rab7-depleted cells, cellular membranes were differentially solubilized with detergents. A short treatment with a low concentration of digitonin should permeabilize only the plasma membrane, while saponin should permeabilize both the plasma membrane and endosomal membranes (Malerød et al., 2007; Villasenor et al., 2016). Therefore, epitopes located inside the lumen of endosomes should be inaccessible for antibodies in cells permeabilized with digitonin but would be readily detected upon saponin treatment. We combined these treatments with the use of antibodies that recognize the cytoplasmic (intracellular) or the luminal (extracellular) part of LTβR (mouse and goat antibodies,

Journal of Cell Science (2018) 131, jcs218883. doi:10.1242/jcs.218883

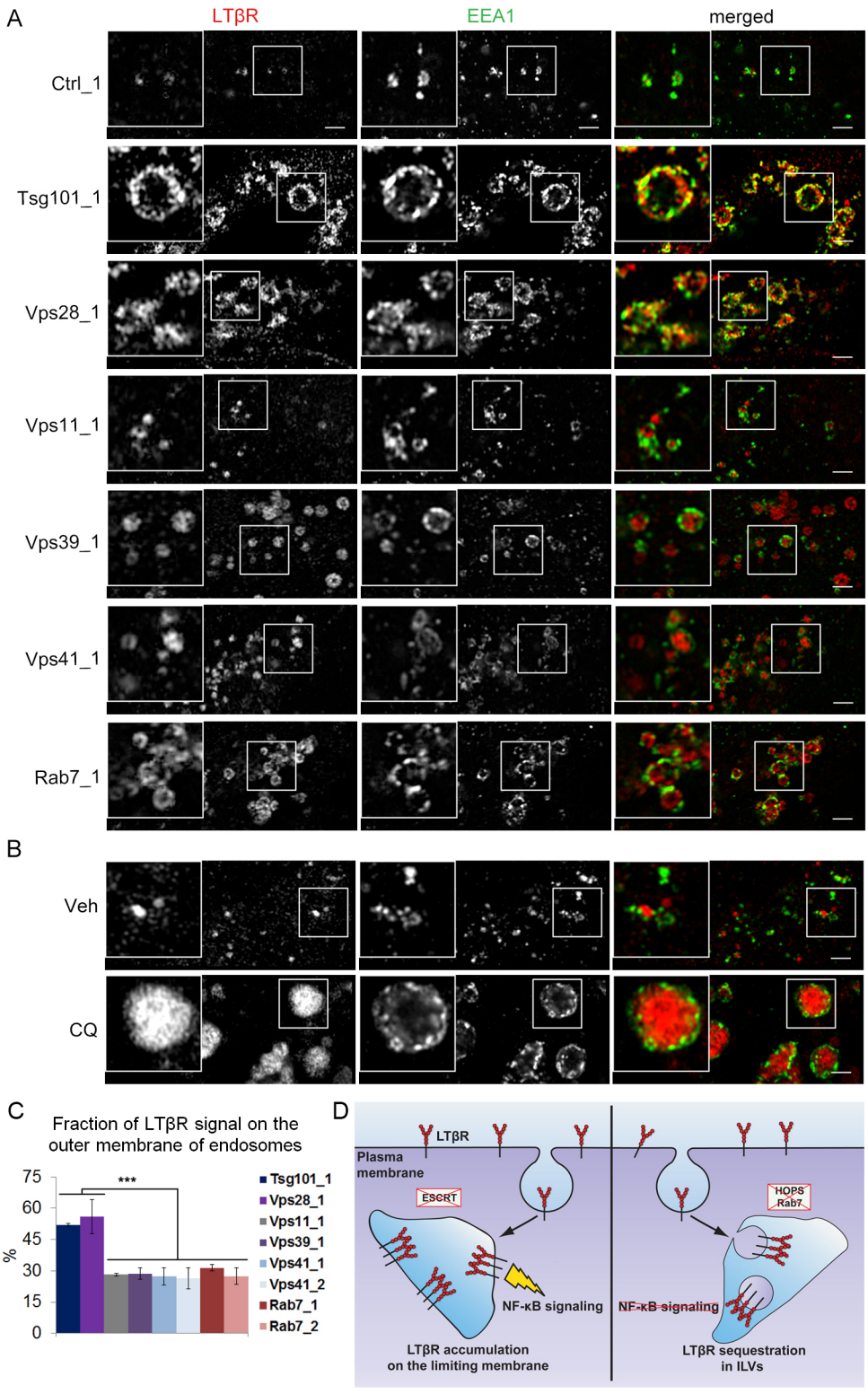

Fig. 6. The topology of LTβR that accumulates on EEA1-positive endosomes in cells depleted of HOPS or that are defective in lysosomal degradation is different from that in ESCRT-I-depleted cells. (A,B) High-resolution images of HeLa cells transfected with siRNAs targeting the indicated ESCRT-I subunits (Tsg101 and Vps28), HOPS components, Rab7 or with control (Ctrl) non-targeting siRNA (A), or cells treated with chloroquine (CQ) or vehicle (Veh) (B). Cells were immunostained for LTβR and EEA1. Insets show magnified views of the regions boxed in the main images. Scale bars: 2 µm. (C) Quantification of the fraction of LTβR signal on the outer membrane of endosomes in cells transfected with siRNAs targeting the indicated ESCRT-I subunits (Tsg101 and Vps28), HOPS components or Rab7 (example images are shown in Fig. S6). The fraction is calculated as the ratio of the integral intensity of vesicular LTβR detected by the antibody recognizing its cytoplasmic tail in digitonin- versus saponin-permeabilized cells. Data represent the means±s.e.m., n=3. ***$P \leq 0.001$ (Mann–Whitney test). (D) Model of the different LTβR topology and signaling upon dysfunction of various trafficking regulators. ESCRT depletion causes LTβR accumulation on the outer membrane of endosomes and activation of NF-κB signaling, while sequestration of LTβR in ILVs upon Rab7 or HOPS depletion prevents the transmission of signals to activate the NF-κB pathway.

respectively). We expected that if LTβR were present predominantly at the outer endosomal membrane, its cytoplasmic tail, but not its luminal part, would be readily detected after digitonin permeabilization. In turn, LTβR sequestered in ILVs would be largely protected from detection by both antibodies after digitonin treatment. In all cases, saponin permeabilization would be expected to allow for efficient detection of both LTβR epitopes. As an additional control, we used an antibody against the cytoplasmic C-terminus of LAMP1, as its staining should not differ in cells treated with digitonin or saponin.

After digitonin permeabilization of ESCRT-depleted cells, we could detect the cytoplasmic tail of LTβR, but not its luminal part (Fig. S6). This indicated that LTβR localized preferentially on the outer membrane of endosomes. By contrast, after digitonin treatment of HOPS- or Rab7-depleted cells, both parts of LTβR

Journal of Cell Science (2018) 131, jcs218883. doi:10.1242/jcs.218883

were poorly detected (Fig. S6). This argues that both LTβR epitopes were protected inside endosomes. We then quantified the integral intensity of the LTβR signal derived from its intracellular tail after digitonin and saponin permeabilization. The comparison of these two values allowed us to estimate the fraction of LTβR exposed on the outer membrane of endosomes. We observed that this fraction was significantly lower in HOPS- or Rab7-depleted cells, consistent with the localization of LTβR in ILVs, when compared to what as seen upon ESCRT knockdown (Fig. 6C). Taken together, these results show that the intraendosomal topology of accumulated LTβR is different in cells depleted of various regulators of endocytic trafficking. This different sub-organellar localization of the receptor further determines its ultimate signaling outcome.

DISCUSSION

Overall, the findings presented in this study shed light on the still poorly characterized trafficking of LTβR and the regulation of ligand-independent NF-κB signaling. We observed strong intracellular accumulation of LTβR on endocytic structures upon depletion of endosomal sorting/tethering complexes or upon chemical inhibition of lysosomal degradation. This indicates that the receptor is constitutively internalized, even in the absence of its ligands. Our present and previous studies (Maminska et al., 2016) suggest that internalized LTβR is trafficked through multivesicular endosomes, formed in an ESCRT-dependent manner, that then mature and fuse with lysosomes in a process regulated by Rab7 and HOPS. Since results obtained in yeast indicate that CORVET and HOPS complexes act sequentially during endosomal transport (Balderhaar and Ungermann, 2013), we were surprised to see no effect of CORVET depletion on LTβR trafficking. Experimental data on the function of mammalian CORVET is still limited; however, recently it has been implicated in integrin recycling (Jonker et al., 2018). Thus, we cannot rule out that, upon CORVET deficiency, fusion of early endosomes can be mediated by other endocytic machineries (Balderhaar et al., 2013). It is also possible that distinct subpopulations of early endosomes harboring various cargoes can cooperate with specific tethering complexes. Moreover, different effects of ESCRT and HOPS depletion on LTβR trafficking and signaling also argue that ESCRT-dependent ILV formation occurs in parallel to and can be uncoupled from HOPS-mediated Rab5-to-Rab7 conversion. While normally these two processes are coordinated in time to ensure proper endosomal transport, their regulatory mechanisms are independent and can be selectively perturbed, with different consequences for cargo trafficking and, possibly, signaling.

With respect to the signaling of LTβR, we discovered that its intraendosomal sequestration in ILVs upon Rab7 or HOPS depletion prevents the transmission of signals to activate the NF-κB pathway, although the receptor is in an active state, bound to the TRAF adaptors (Fig. 6D). This is in contrast to the accumulation of LTβR-TRAF complexes on the outer membrane of endosomes that is seen upon ESCRT depletion and activates NF-κB signaling (Maminska et al., 2016). The concept of intraendosomal sequestration of signaling molecules has already been proposed for the canonical Wnt pathway, where the negative regulator GSK3β was enclosed in ILVs upon ligand stimulation, thus allowing for signal transduction (Dobrowolski et al., 2012; Taelman et al., 2010). In our case, active LTβR–TRAF complexes, formed in the absence of ligand stimulation, are incorporated into ILVs that inhibits signaling. Previous studies have reported that TRAF2 can indeed undergo lysosomal degradation upon ligand-induced NF-κB activation (Varfolomeev et al., 2012; Vince et al., 2008). However, our findings refer to ligand-free conditions and, in this context, it was surprising to detect a substantial LTβR–TRAF interaction upon inhibition of lysosomal degradation through Rab7 depletion or chloroquine treatment (Figs 4A and 5F). This poses a question of where and when this association forms, as it requires recruitment of TRAFs from the cytoplasm and is expected to occur before the incorporation of LTβR into ILVs. In control cells, we detected limited binding between LTβR and TRAFs. This may suggest that, in the steady-state, a certain proportion of LTβR could be activated (e.g. due to stochastic or regulated clustering and proximity-driven oligomerization) and recruit TRAFs at the plasma membrane and/or endosomes. However, owing to constitutive internalization of the receptor, such LTβR–TRAF complexes would be efficiently enclosed inside ILVs and subsequently degraded, thereby preventing their signaling. Now, we show that trafficking deficiencies can lead to the build-up of LTβR–TRAF complexes that can signal to NF-κB if they have accumulated on the outer membrane of endosomes and are exposed to the cytoplasm (upon ESCRT depletion) but cannot signal when incorporated into ILVs (upon Rab7 or HOPS depletion, or chloroquine treatment) (Fig. 6D).

Generally, our study demonstrates that endosomal sorting and transport represents a regulatory mechanism to limit NF-κB signaling or prevent its spurious induction in the absence of exogenous stimulation. On the other hand, NF-κB activation initiated by LTβR and other cytokine receptors accumulated on endosomes upon trafficking defects can be considered as a signal of organellar dysfunction. We discovered that such intracellularly induced inflammatory response critically depends on the exact endosomal sorting defect and the resulting topology of cytokine receptors within the endosomal compartments.

MATERIALS AND METHODS

Cell culture

HeLa, HEK 293 and HEK 293T cells were purchased from ATCC and later authenticated as required. HeLa cells were maintained in high-glucose modified Eagle's medium (MEM), HEK 293 and HEK 293T cells were grown in high-glucose Dulbecco's modified Eagle's medium (DMEM) (Sigma-Aldrich), and both media were supplemented with 10% fetal bovine serum (FBS) and 2 mM L-glutamine (Sigma-Aldrich). Cells were routinely tested for mycoplasma contamination. Chloroquine (Sigma-Aldrich) was used at 100 µM concentration for 20 h. For analysis of transferrin and EGF internalization, HeLa cells were serum-starved overnight and then stimulated for 15 min in serum-free medium with 25 µg/ml transferrin labeled with Alexa Fluor 647 (T23366) and 100 ng/ml biotinylated EGF conjugated to Alexa Fluor 555–streptavidin (E35350) from ThermoFisher Scientific.

Antibodies

Primary antibodies used for western blotting were: rabbit anti-Vps11 (19140-1-AP, 1:600) and anti-Vps41 (13869-1-AP, 1:200) from ProteinTech; rabbit anti-GAPDH (sc-25778, 1:2000), rabbit anti-TRAF3 (sc-949, 1:500) and goat anti-LTβR (sc-8375, 1:500) from Santa Cruz Biotechnology; mouse anti-vinculin (V9131, 1:5000) from Sigma-Aldrich; rabbit anti-p100/p52 (4882S), rabbit anti-phospho-Akt (9271S), mouse anti-Akt (2920S), rabbit anti-phospho-Erk1/2 (9101S), mouse anti-Erk1/2 (9107S), mouse anti-IκBα (4814S), mouse anti-phospho-JNK (9255S), rabbit anti-JNK (9252S), rabbit anti-phospho-RelA (3033), mouse anti-RelA (6956S) and rabbit anti-Rab7 (9367) from Cell Signaling Technology, all diluted 1:1000; rabbit anti-Vps28 (ab167172, 1:1000) from Abcam; and mouse anti-TRAF2 (558890, 1:1000) from BD Biosciences.

Primary antibodies used for immunofluorescence were: rabbit anti-EEA1 (ALX-210-239, 1:400) from Enzo Life Sciences; rabbit anti-HA (sc-805, 1:200) from Santa Cruz Biotechnology; agonistic goat anti-LTβR (AF629, 1:200) from R&D Systems; mouse anti-LTβR (H00004055-B01P, 1:200) from Abnova, rabbit anti-LAMP1 (L-1418, 1:400) from Sigma-Aldrich, and mouse anti-LAMP1 (H4A3, IF 1:800) developed by J. Thomas August and

James E.K. Hildreth from the Developmental Studies Hybridoma Bank developed under the auspices of the NICHD and maintained by the University of Iowa, Department of Biology, Iowa City, Iowa, USA.

Secondary horseradish peroxidase (HRP)-conjugated anti-mouse-IgG (111-035-062), anti-rabbit-IgG (111-035-144) and anti-goat-IgG (805-035-180) antibodies were from Jackson ImmunoResearch; secondary fluorophore-conjugated anti-rabbit-IgG conjugated to IRDye 680 (926-68023) and anti-mouse-IgG conjugated to IRDye 800CW (926-32212) antibodies used in the Odyssey system were from LICOR Biosciences. Secondary antibodies used for immunofluorescence were: Alexa Fluor 488-, 555-, 647-conjugated anti-goat-IgG, anti-mouse-IgG and anti-rabbit-IgG were from ThermoFisher Scientific. All secondary antibodies were diluted 1:10,000.

For the immunoprecipitation assay, goat agonistic anti-LTβR (AF629, R&D Systems) and control goat IgG (I5256, Sigma-Aldrich) were used.

Immunofluorescence staining and image analysis

Routinely, cells were transferred onto ice, washed twice with ice-cold PBS, and fixed with ice-cold 3% paraformaldehyde (PFA) for 15 min. After three washes with PBS, cells were processed directly for immunostaining, as described previously (Jastrzebski et al., 2017; Maminska et al., 2016; Sadowski et al., 2013).

To discriminate between LTβR exposed on the surface of endosomes from that sequestered inside ILVs, we used differential detergent solubilization as previously described (Malerød et al., 2007; Villasenor et al., 2016). Cells were fixed with 3% PFA for 7 min and permeabilized with 0.1% saponin (Sigma-Aldrich) for 10 min or with 0.001% digitonin (Abcam) for 1 min, washed twice with PBS and blocked for 30 min with 5 mg/ml BSA (Bioshop) and 0.2% gelatin from cold-water fish skin (Sigma-Aldrich). Then cells were incubated for 1 h with mouse anti-LTβR, agonistic goat antibody against LTβR and rabbit anti-LAMP1 antibody. From this step, samples were processed as described previously (Jastrzebski et al., 2017; Maminska et al., 2016; Sadowski et al., 2013).

Slides were scanned using a ZEISS LSM 710 confocal microscope with an EC Plan-Neofluar 40×1.3 NA oil immersion objective. ZEN 2009 software (Zeiss) was used for image acquisition. At least ten 12-bit images with a resolution of 1024×1024 pixels were acquired per experimental condition. Images were imported into MotionTracking (http://motiontracking.mpi-cbg.de) to analyze the integral intensity or mean of integral intensity of fluorescence of LTβR in all vesicles (expressed in arbitrary units, AU) and the percentage of colocalization between two or three markers (Collinet et al., 2010; Kalaidzidis et al., 2015; Rink et al., 2005). Pictures were assembled in Photoshop (Adobe) with only linear adjustments of contrast and brightness.

Airyscan imaging and processing

Airyscan imaging was performed with a confocal laser scanning microscope ZEISS LSM 800 equipped with Plan-Apochromat 63×/1.40 NA oil objective and an Airyscan detection unit, using Immersol 518 F immersion medium (Zeiss). Detector gain and pixel dwell times were adjusted for each dataset, keeping them at their lowest values to avoid saturation and bleaching effects. ZEN Blue 2.3 (Version 2.3.69.1003) software (Zeiss) was used for image acquisition. The Airyscan processing module with default settings was used to process obtained data. Pictures were assembled in Photoshop (Adobe) with only linear adjustments of contrast and brightness.

Transfection with siRNAs

siRNA transfections were performed according to manufacturers' instructions using RNAiMAX (ThermoFisher Scientific) in HeLa cells or HiPerFect in HEK 293 cells (Qiagen). HeLa cells were seeded on the same day as transfection on 12 mm coverslips in a 24-well plate (4×10^4 cells/well) for microscopy experiments, on a 12-well plate for qRT-PCR and western blotting (7.5×10^4 cells/well) or on a 10 cm dish for immunoprecipitation experiments (1.1×10^6 cells/plate). HEK 293 cells were seeded 1 day before transfection in six-well plates (8×10^5 cells/well) for microarray analysis. Cells were analyzed 72 h (HOPS-, CORVET- and Rab7-depleted cells) or 48 h (Vps28- and Tsg101-depleted cells) post transfection. For microarray analysis, total RNA was isolated from HEK 293 cells 72 h after transfection. The concentration of siRNA in HeLa cells was 10 nM, except siRNAs targeting Tsg101 and Vps28 (2 nM) or Vps3 and Vps8 (20 nM). The concentration of siRNA in HEK 293 cells was 15 nM. The following Ambion Silencer Select siRNAs (ThermoFisher Scientific) were used: Ctrl_1 (Negative Control No. 1, 4390843), Ctrl_2 (Negative Control No. 2, 4390846), Rab7_1 (s15442), Rab7_2 (s15444), Tsg101_1 (s14440), Vps3_1 (s17973), Vps3_2 (s17974), Vps8_1 (s23635), Vps8_2 (s23637), Vps11_1 (s31595), Vps11_2 (s31597), Vps11_3 (s31596), Vps16_1 (s34802), Vps16_2 (s34803), Vps18_1 (s33451), Vps18_2 (s33453), Vps28_1 (s27579), Vps28_2 (s27577), Vps39_1 (s23601), Vps39_2 (s23599), Vps41_1 (s25768) and Vps41_2 (s25770).

Generation of Vps39- and Vps41-knockout HeLa cell lines by CRISPR/Cas9

Genome editing of HeLa cells was performed using a double-nicking strategy to knockout *VPS39* and *VPS41*. For each gene, two 20-bp-long single-guide RNA (sgRNAs) were designed based on the Brunello library (Doench et al., 2016). To clone sgRNAs, BsmBI recognition sites were appended along with the appropriate overhang sequences to each pair of the oligonucleotides (Table S1), that then were annealed and ligated with gRNA expression LentiCRISPR v2 vector (Addgene vector #52961).

The sgRNA plasmids (4 µg) along with pPAX2 (3 µg) and pMD2.G (1 µg) were used for transfection of HEK 293T cells plated into six-well plates (8×10^5 cells/well) to produce lentiviruses. At 48 h post transfection, HeLa cells (plated 1 day before in six-well format at 1.25×10^5 cells/well) were infected with the harvested viruses and grown for 2 days before addition of puromycin (1.2 µg/ml). After 10 days of selection for puromycin resistance, cells were plated in medium without antibiotic and analyzed.

Generation of Rab7 depletion in HeLa cells with shRNA

Small hairpin RNA (shRNA) targeting Rab7a (primer sequence: forward, 5′-CCGGGTGTTGCTGAAGGTTATCACTGCAGTGATAACCTTCAG-CAACA- CTTTTTG-3′; reverse 5′-AATTCAAAAAGTGTTGCTGAAG-GTTATCACTGCAGTGATAACCTTCAGCAACAC-3′) was cloned into lentiviral vector pLKO.1 TRC cloning vector (Addgene #10878). Lentiviral vectors pLKO.1 - TRC control (Addgene #10879) and scramble shRNA (Addgene #1864) were used as controls. The shRNA plasmids (4 µg) along with pPAX2 (3 µg) and pMD2.G (1 µg) were used for transfection of HEK 293T cells plated into six-well plates (8×10^5 cells/well) to produce lentiviruses. At 48 h post transfection, HeLa cells (plated 1 day before in six-well format at 10^5 cells/well) were infected with the harvested viruses and grown for 2 days before selection for puromycin resistance (1 µg/ml). After 7 days of selection, cells were plated in medium without antibiotic and analyzed.

Rab7 rescue experiment

HeLa cells (4×10^4 cells/well in 24-well format) were transfected with 10 nM siRNA against Rab7 or control siRNA. After 24 h, cells were transfected with 0.5 µg of plasmid encoding canine Rab7a protein (pcDNA3 HA-Rab7a, gift from Prof. Cecilia Bucci, Department of Biological and Environmental Sciences and Technologies, University of Salento, Italy) or control pcDNA3-HA-NI (gift from Prof. Kazuhisa Nakayama, Department of Physiological Chemistry, Kyoto University, Japan) using FuGENE 6 (Promega) according to manufacturer's instructions. The nucleotide sequence of canine Rab7a construct is resistant to silencing with Rab7_2 siRNA (two nucleotide mismatches) but not Rab7_1 siRNA (complete match). After 72 h (starting from the transfection with siRNA), cells were fixed with paraformaldehyde and analyzed by immunofluorescence staining as described above.

Western blotting

HeLa cells were lysed in RIPA buffer (1% Triton X-100, 0.5% sodium deoxycholate, 0.1% SDS, 50 mM Tris-HCl pH 7.4, 150 mM NaCl, 0.5 mM EDTA) supplemented with protease inhibitor cocktail (6 µg/ml chymostatin, 0.5 µg/ml leupeptin, 10 µg/ml antipain, 2 µg/ml aprotinin, 0.7 µg/ml pepstatin A and 10 µg/ml 4-amidinophenylmethanesulfonyl fluoride hydrochloride; Sigma-Aldrich) and phosphatase inhibitor cocktails (Sigma-Aldrich, P0044 and P5726). Protein concentration was measured with the BCA protein assay

kit (ThermoFisher Scientific). A total of 10–50 µg protein per sample was resolved by SDS-PAGE, transferred to nitrocellulose membrane (Whatman), probed with specific primary and secondary antibodies, and detected by using the ChemiDoc imaging system (Bio-Rad) or Odyssey infrared imaging system (LI-COR Biosciences). Densitometry of protein bands was carried out using ImageJ Software (Schneider et al., 2012).

Immunoprecipitation

HeLa cell lysates were prepared in RIPA buffer. 250-500 µg of protein was used per reaction. Cell extracts were diluted in immunoprecipitation (IP) buffer (50 mM HEPES, pH 7.5, 150 mM NaCl, 1 mM EGTA, 1 mM EDTA, 1% Triton X-100, 10% glycerol, 5 µg/ml DNase and protease inhibitor cocktail) and pre-cleared for 3 h at 4°C with goat IgG (Sigma-Aldrich) and Protein G–agarose beads (Roche) to deplete nonspecifically bound proteins. Pre-cleared cell lysates were incubated overnight at 4°C with 2.5 µg of antibodies (specific anti-LTβR or unspecific goat IgG) with constant rotation. Immune complexes were recovered by a 2 h incubation with Protein G–agarose beads at 4°C with rotation. The agarose beads with bound protein complexes were spun down and washed four times using IP buffer. Next, samples were incubated at 95°C for 10 min with Laemmli buffer and subjected to electrophoresis on 10% polyacrylamide gels.

Quantitative real-time PCR

Total RNA was isolated with a High Pure Isolation Kit (Roche). For cDNA synthesis, random nonamers, oligo(dT)23 and M-MLV reverse transcriptase (Sigma-Aldrich) were used according to manufacturer's instructions. To estimate the expression of genes of interest we used primers designed with the NCBI tool (and custom-synthesized by Sigma-Aldrich) as listed in Table S2 or TaqMan® Gene Expression Assays (ThermoFisher Scientific) as listed in Table S3.

The qRT-PCR was performed with the KAPA SYBR FAST qPCR Master Mix (2X) Universal Kit (KK4618, KapaBiosystems) or TaqMan® Gene Expression Master Mix (4369016, ThermoFisher Scientific) using a 7900HT Fast Real-Time PCR thermocycler (Applied Biosystems) with at least two technical repeats per experimental condition. The data were normalized according to the level of housekeeping genes *ACTB*, *B2M*, and *GAPDH* and presented as fold changes.

Microarray analysis

HEK 293 cells were transfected with control (Ctrl_1 or Ctrl_2) or HOPS-targeting (Vps11_1, Vps39_1, Vps39_2, Vps41_1 or Vps41_2) siRNAs in three biological repetitions (21 samples in total). A starting amount of 200 ng of high-quality total RNA was used to generate cDNA and cRNA with the Illumina TotalPrep RNA Amplification Kit (Illumina). The cRNA samples were prepared according to a procedure described elsewhere (Pera et al., 2013). Each cRNA sample (1.5 µg) was hybridized overnight to the Human HT-12 BeadChip array (Illumina) in a multiple-step procedure; the chips were washed, dried and scanned on the BeadArray Reader (Illumina). Raw microarray data were generated using BeadStudio v3.0 (Illumina). A total of 21 Illumina HumanHT-12v4 microarrays were used in the experiment. To provide an appropriate balance in the entire data set, the groups were equally divided between the array plates and the hybridization batches. Microarray analysis and quality control of the arrays were performed with BeadArray R package v1.10.0 software. After background subtraction (using the median background method), the data were normalized by quantile normalization and were subsequently $\log_2$ transformed. The obtained signal was taken as the measure of mRNA abundance derived from the level of gene (or its particular transcriptional variant) expression.

Statistical analysis of the results was performed using a *t*-test followed by correction for multiple testing using false discovery rate (FDR). The FDR was estimated using the Benjamini and Hochberg method. All statistical analyses were performed using R software (https://www.r-project.org/).

Differentially expressed genes were investigated for putative cellular functions. Overrepresented functional groups of genes were obtained from the gene ontology (GO) DAVID 6.7 database at http://david.abcc.ncifcrf.gov (Huang da et al., 2009).

Statistical analysis

At least three independent experiments were performed in each case. Statistical testing was performed using Prism 6 (GraphPad Software). Data were analyzed for Gaussian distribution with a Kolmogorov–Smirnov test with the Dallal–Wilkinson–Lilliefor corrected *P* value. In case of Gaussian distribution, a parametric Student's *t*-test or one-way ANOVA with Dunnett's post-hoc test was used as appropriate. In case of non-Gaussian distribution, a nonparametric Mann–Whitney or Kruskal–Wallis with Dunn's post-hoc test was used. The significance of mean comparison is annotated as follows: ns, non-significant ($P>0.05$), *$P\leq0.05$, **$P\leq0.01$, and ***$P\leq0.001$. No statistical methods were used to predetermine sample size.

Acknowledgements

We thank the Miaczynska laboratory members for critical reading of the manuscript. We would like to thank Ewa Liszewska for help with shRNA construct preparation, and to Małgorzata Świątek, Renata Wyszyńska and Michał Liput for technical assistance.

Competing interests

The authors declare no competing or financial interests.

Author contributions

Conceptualization: M.B.-O., K.J., M. Miaczynska; Methodology: M.B.-O., K.J., J.C., M. Maksymowicz, K.W., M.K., D.M.; Formal analysis: M.B.-O., K.J., J.C., M.K., D.M.; Investigation: M.B.-O., K.J., J.C., M. Maksymowicz, K.W.; Resources: M.K., D.M., J.G.; Writing - original draft: M.B.-O., K.J., M. Miaczynska; Writing - review & editing: M.B.-O., K.J., J.C., M. Maksymowicz, K.W., D.M., J.G., M. Miaczynska; Supervision: J.G., M. Miaczynska; Project administration: M. Miaczynska; Funding acquisition: M.B.-O., J.G., M. Miaczynska.

Precise contributions are as follows: M.B.-O. designed, performed and analyzed experiments in Fig. 2E,F; Fig. 3E; Fig. 4; Fig. 5E,F; Fig. S2; Figs S3C, S4A, D; Fig. S5A and wrote the manuscript; K.J. designed, performed and analyzed experiments in Fig. 1A–D; Fig. 2A,D; Fig. 3A–D,F-G; Figs 5A–D, 6A–C, Fig. S1A,B, D; Figs S2, S3A,B, S6 and wrote the manuscript; J.C. designed, performed and analyzed experiments in Fig. S5C–E; M. Maksymowicz contributed data to Fig. 2F; Fig. 4B,C; Fig. 5A–D; Fig. S2E and performed experiments in Fig. S4B,C; K.W. contributed data to Fig. 1E; Fig. 5A–D; Fig. S1C; Fig. S2E,F; M.K. performed the microarray analysis; D.M. and J.G. contributed to design and analysis of experiments; M. Miaczynska conceived, designed and analyzed experiments and wrote the manuscript.

Funding

This work was supported from the Narodowe Centrum Nauki (National Science Center) by a MAESTRO grant (UMO-2011/02/A/NZ3/00149) to M. Miaczynska and by a grant from Switzerland through the Swiss Contribution to the enlarged European Union (Polish-Swiss Research Programme project PSPB-094/2010) to M. Miaczynska and J.G. M.B.-O. and M. Maksymowicz were supported by OPUS grant (UMO-2016/21/B/NZ3/03637) from the National Science Center. J.C. and K.W. were supported by HOMING grant (Homing/2016-1/1) and the TEAM programme (TEAM/2016-2/15, to M. Miaczynska), respectively, both from the Foundation for Polish Science co-financed by the European Union under the European Regional Development Fund.

Supplementary information

Supplementary information available online at
http://jcs.biologists.org/lookup/doi/10.1242/jcs.218883.supplemental

References

Balderhaar, H. J. and Ungermann, C. (2013). CORVET and HOPS tethering complexes-coordinators of endosome and lysosome fusion. *J. Cell Sci.* **126**, 1307-1316.

Balderhaar, H. J., Lachmann, J., Yavavli, E., Brocker, C., Lurick, A. and Ungermann, C. (2013). The CORVET complex promotes tethering and fusion of Rab5/Vps21-positive membranes. *Proc. Natl. Acad. Sci. USA* **110**, 3823-3828.

Barbieri, E., Di Fiore, P. P. and Sigismund, S. (2016). Endocytic control of signaling at the plasma membrane. *Curr. Opin. Cell Biol.* **39**, 21-27.

Brankatschk, B., Wichert, S. P., Johnson, S. D., Schaad, O., Rossner, M. J. and Gruenberg, J. (2012). Regulation of the EGF transcriptional response by endocytic sorting. *Sci. Signal.* **5**, ra21.

Cendrowski, J., Mamińska, A. and Miaczynska, M. (2016). Endocytic regulation of cytokine receptor signaling. *Cytokine Growth Factor. Rev.* **32**, 63-73.

Chang, Y. H., Hsieh, S. L., Chen, M. C. and Lin, W. W. (2002). Lymphotoxin beta receptor induces interleukin 8 gene expression via NF-kappaB and AP-1 activation. *Exp. Cell Res.* **278**, 166-174.

Christ, L., Raiborg, C., Wenzel, E. M., Campsteijn, C. and Stenmark, H. (2017). Cellular functions and molecular mechanisms of the ESCRT membrane-scission machinery. *Trends Biochem. Sci.* **42**, 42-56.

Collinet, C., Stöter, M., Bradshaw, C. R., Samusik, N., Rink, J. C., Kenski, D., Habermann, B., Buchholz, F., Henschel, R., Mueller, M. S. et al. (2010). Systems survey of endocytosis by multiparametric image analysis. *Nature* **464**, 243-249.

Dejardin, E., Droin, N. M., Delhase, M., Haas, E., Cao, Y., Makris, C., Li, Z.-W., Karin, M., Ware, C. F. and Green, D. R. (2002). The lymphotoxin-beta receptor induces different patterns of gene expression via two NF-kappaB pathways. *Immunity* **17**, 525-535.

Dobrowolski, R., Vick, P., Ploper, D., Gumper, I., Snitkin, H., Sabatini, D. D. and De Robertis, E. M. (2012). Presenilin deficiency or lysosomal inhibition enhances Wnt signaling through relocalization of GSK3 to the late-endosomal compartment. *Cell Rep* **2**, 1316-1328.

Doench, J. G., Fusi, N., Sullender, M., Hegde, M., Vaimberg, E. W., Donovan, K. F., Smith, I., Tothova, Z., Wilen, C., Orchard, R. et al. (2016). Optimized sgRNA design to maximize activity and minimize off-target effects of CRISPR-Cas9. *Nat. Biotechnol.* **34**, 184-191.

Frankel, E. B. and Audhya, A. (2018). ESCRT-dependent cargo sorting at multivesicular endosomes. *Semin. Cell Dev. Biol.* **74**, 4-10.

Ganeff, C., Remouchamps, C., Boutaffala, L., Benezech, C., Galopin, G., Vandepaer, S., Bouillenne, F., Ormenese, S., Chariot, A., Schneider, P. et al. (2011). Induction of the alternative NF-kappaB pathway by lymphotoxin alphabeta (LTalphabeta) relies on internalization of LTbeta receptor. *Mol. Cell. Biol.* **31**, 4319-4334.

Guerra, F. and Bucci, C. (2016). Multiple roles of the small GTPase Rab7. *Cells* **5**, E34.

Huang da, W., Sherman, B. T. and Lempicki, R. A. (2009). Systematic and integrative analysis of large gene lists using DAVID bioinformatics resources. *Nat. Protoc.* **4**, 44-57.

Huotari, J. and Helenius, A. (2011). Endosome maturation. *EMBO J.* **30**, 3481-3500.

Jastrzebski, K., Zdzalik-Bielecka, D., Maminska, A., Kalaidzidis, Y., Hellberg, C. and Miaczynska, M. (2017). Multiple routes of endocytic internalization of PDGFRbeta contribute to PDGF-induced STAT3 signaling. *J. Cell Sci.* **130**, 577-589.

Jonker, C. T. H., Galmes, R., Veenendaal, T., Ten Brink, C., van der Welle, R. E. N., Liv, N., de Rooij, J., Peden, A. A., van der Sluijs, P., Margadant, C. et al. (2018). Vps3 and Vps8 control integrin trafficking from early to recycling endosomes and regulate integrin-dependent functions. *Nat. Commun.* **9**, 792.

Kalaidzidis, Y., Kalaidzidis, I. and Zerial, M. (2015). A probabilistic method to quantify the colocalization of markers on intracellular vesicular structures visualized by light microscopy. *Bayesian Inference and Maximum Entropy Methods in Science and Engineering (Maxent 2014)* **1641**, 580-587.

Khatter, D., Raina, V. B., Dwivedi, D., Sindhwani, A., Bahl, S. and Sharma, M. (2015). The small GTPase Arl8b regulates assembly of the mammalian HOPS complex on lysosomes. *J. Cell Sci.* **128**, 1746-1761.

Kim, Y.-S., Nedospasov, S. A. and Liu, Z. G. (2005). TRAF2 plays a key, nonredundant role in LIGHT-lymphotoxin beta receptor signaling. *Mol. Cell. Biol.* **25**, 2130-2137.

Lin, X., Yang, T., Wang, S., Wang, Z., Yun, Y., Sun, L., Zhou, Y., Xu, X., Akazawa, C., Hong, W. et al. (2014). RILP interacts with HOPS complex via VPS41 subunit to regulate endocytic trafficking. *Sci. Rep.* **4**, 7282.

Malerød, L., Stuffers, S., Brech, A. and Stenmark, H. (2007). Vps22/EAP30 in ESCRT-II mediates endosomal sorting of growth factor and chemokine receptors destined for lysosomal degradation. *Traffic* **8**, 1617-1629.

Maminska, A., Bartosik, A., Banach-Orlowska, M., Pilecka, I., Jastrzebski, K., Zdzalik-Bielecka, D., Castanon, I., Poulain, M., Neyen, C., Wolinska-Niziol, L. et al. (2016). ESCRT proteins restrict constitutive NF-kappaB signaling by trafficking cytokine receptors. *Sci. Signal.* **9**, ra8.

Markgraf, D. F., Ahnert, F., Arlt, H., Mari, M., Peplowska, K., Epp, N., Griffith, J., Reggiori, F. and Ungermann, C. (2009). The CORVET subunit Vps8 cooperates with the Rab5 homolog Vps21 to induce clustering of late endosomal compartments. *Mol. Biol. Cell* **20**, 5276-5289.

Miaczynska, M. (2013). Effects of membrane trafficking on signaling by receptor tyrosine kinases. *Cold Spring Harb. Perspect. Biol.* **5**, a009035.

Müller, J. R. and Siebenlist, U. (2003). Lymphotoxin beta receptor induces sequential activation of distinct NF-kappa B factors via separate signaling pathways. *J. Biol. Chem.* **278**, 12006-12012.

Nakano, H., Oshima, H., Chung, W., Williams-Abbott, L., Ware, C. F., Yagita, H. and Okumura, K. (1996). TRAF5, an activator of NF-kappaB and putative signal transducer for the lymphotoxin-beta receptor. *J. Biol. Chem.* **271**, 14661-14664.

Peplowska, K., Markgraf, D. F., Ostrowicz, C. W., Bange, G. and Ungermann, C. (2007). The CORVET tethering complex interacts with the yeast Rab5 homolog Vps21 and is involved in endo-lysosomal biogenesis. *Dev. Cell* **12**, 739-750.

Pera, J., Korostynski, M., Golda, S., Piechota, M., Dzbek, J., Krzyszkowski, T., Dziedzic, T., Moskala, M., Przewlocki, R., Szczudlik, A. et al. (2013). Gene expression profiling of blood in ruptured intracranial aneurysms: in search of biomarkers. *J. Cereb. Blood Flow Metab.* **33**, 1025-1031.

Perini, E. D., Schaefer, R., Stöter, M., Kalaidzidis, Y. and Zerial, M. (2014). Mammalian CORVET is required for fusion and conversion of distinct early endosome subpopulations. *Traffic* **15**, 1366-1389.

Poteryaev, D., Datta, S., Ackema, K., Zerial, M. and Spang, A. (2010). Identification of the switch in early-to-late endosome transition. *Cell* **141**, 497-508.

Price, A., Seals, D., Wickner, W. and Ungermann, C. (2000). The docking stage of yeast vacuole fusion requires the transfer of proteins from a cis-SNARE complex to a Rab/Ypt protein. *J. Cell Biol.* **148**, 1231-1238.

Remouchamps, C., Boutaffala, L., Ganeff, C. and Dejardin, E. (2011). Biology and signal transduction pathways of the Lymphotoxin-alphabeta/LTbetaR system. *Cytokine Growth Factor. Rev.* **22**, 301-310.

Rink, J., Ghigo, E., Kalaidzidis, Y. and Zerial, M. (2005). Rab conversion as a mechanism of progression from early to late endosomes. *Cell* **122**, 735-749.

Sadowski, Ł., Jastrzębski, K., Kalaidzidis, Y., Heldin, C.-H., Hellberg, C. and Miaczynska, M. (2013). Dynamin inhibitors impair endocytosis and mitogenic signaling of PDGF. *Traffic* **14**, 725-736.

Schneider, C. A., Rasband, W. S. and Eliceiri, K. W. (2012). NIH Image to ImageJ: 25 years of image analysis. *Nat. Methods* **9**, 671-675.

Scott, C. C., Vacca, F. and Gruenberg, J. (2014). Endosome maturation, transport and functions. *Semin. Cell Dev. Biol.* **31**, 2-10.

Spang, A. (2016). Membrane tethering complexes in the endosomal system. *Front. Cell Dev. Biol.* **4**, 35.

Szymanska, E., Budick-Harmelin, N. and Miaczynska, M. (2018). Endosomal "sort" of signaling control: The role of ESCRT machinery in regulation of receptor-mediated signaling pathways. *Semin. Cell Dev. Biol.* **74**, 11-20.

Taelman, V. F., Dobrowolski, R., Plouhinec, J.-L., Fuentealba, L. C., Vorwald, P. P., Gumper, I., Sabatini, D. D. and De Robertis, E. M. (2010). Wnt signaling requires sequestration of glycogen synthase kinase 3 inside multivesicular endosomes. *Cell* **143**, 1136-1148.

VanArsdale, T. L., VanArsdale, S. L., Force, W. R., Walter, B. N., Mosialos, G., Kieff, E., Reed, J. C. and Ware, C. F. (1997). Lymphotoxin-beta receptor signaling complex: role of tumor necrosis factor receptor-associated factor 3 recruitment in cell death and activation of nuclear factor kappaB. *Proc. Natl. Acad. Sci. USA* **94**, 2460-2465.

Varfolomeev, E., Goncharov, T., Maecker, H., Zobel, K., Komuves, L. G., Deshayes, K. and Vucic, D. (2012). Cellular inhibitors of apoptosis are global regulators of NF-kappaB and MAPK activation by members of the TNF family of receptors. *Sci. Signal.* **5**, ra22.

Villasenor, R., Kalaidzidis, Y. and Zerial, M. (2016). Signal processing by the endosomal system. *Curr. Opin. Cell Biol.* **39**, 53-60.

Vince, J. E., Chau, D., Callus, B., Wong, W. W.-L., Hawkins, C. J., Schneider, P., McKinlay, M., Benetatos, C. A., Condon, S. M., Chunduru, S. K. et al. (2008). TWEAK-FN14 signaling induces lysosomal degradation of a cIAP1-TRAF2 complex to sensitize tumor cells to TNFalpha. *J. Cell Biol.* **182**, 171-184.

Zhang, Q., Lenardo, M. J. and Baltimore, D. (2017). 30 Years of NF-kappaB: A Blossoming of Relevance to Human Pathobiology. *Cell* **168**, 37-57.